Chinese Journal of Chemical Engineering 85 (2025) 167–181

Contents lists available at ScienceDirect

Chinese Journal of Chemical Engineering

journal homepage: www.elsevier.com/locate/CJChE

Full Length Article

Optimization of methanol–vinyl acetate azeotrope separation process based on the pressure swing distillation and energy saving study

Xuefeng Feng [1,2], Huiqin Zhou [1,2], Yi Zhang [1,2], Shaolan Zhuang [1,2], Zhongwei Ding [1,2], Qunsheng Li [1,2,*], Yuxin Li [3,4,*]

[1] State Key Laboratory of Chemical Resource Engineering, Beijing University of Chemical Technology, Beijing 100029, China
[2] Engineering Research Center of Preparation Technology of Ultra-Pure Chemicals for Integrated Circuits, Ministry of Education, Beijing University of Chemical Technology, Beijing 100029, China
[3] College of Basic Medical Science, Inner Mongolia Medical University, Inner Mongolia Key Lab of Molecular Biology, Hohhot 010059, China
[4] Inner Mongolia Algal Life Science Co., LTD, Ulanqab 011800, China

ARTICLE INFO

Article history:
Received 12 March 2025
Received in revised form
30 May 2025
Accepted 2 June 2025
Available online 13 June 2025

Keywords:
Pressure swing distillation (PSD)
Methanol–vinyl acetate (VAC) azeotrope
Energy-saving potential
Aspen Plus simulation
Total annual cost (TAC)

ABSTRACT

This study delves into the optimization of the methanol–vinyl acetate (VAC) azeotrope separation process *via* pressure swing distillation (PSD), along with an evaluation of its energy-saving potential. The methanol–VAC system, a polar azeotrope highly susceptible to pressure variations, presents notable separation complexities in polyvinyl alcohol production. Aspen Plus simulations were utilized to assess the feasibility of PSD, with particular emphasis on critical process parameters such as the number of theoretical plates, feed position, reflux ratio, and sidestream extraction location. The results indicate that PSD demonstrates remarkable efficacy in separating methanol and VAC, achieving purities of 99.88% and 99.73% respectively. When compared to extractive distillation, PSD achieves a reduction of 9.07 $t \cdot h^{-1}$ in steam consumption and minimizes wastewater generation by 20.77 $t \cdot h^{-1}$. Furthermore, the economic assessment reveals a 7.91% decrease in the total annual cost associated with PSD. This study not only provides theoretical insights but also offers practical guidance for the design of energy-efficient and sustainable separation processes. Future research will focus on extending the analysis to encompass multi-pressure scenarios, further enhancing the applicability and robustness of the findings.

1. Introduction

Poly(vinyl alcohol) (PVA), a water-soluble polymer with broad industrial applications, is a critical raw material for polymer chemistry [1,2]. Over five decades, China has emerged as the world's leading PVA producer, employing diverse synthesis pathways such as petroleum-based ethylene, natural gas acetylene, and calcium carbide acetylene [3,4]. The primary distinction among these methods lies in vinyl acetate (VAC) monomer synthesis, with VAC polymerization predominantly conducted *via* solution polymerization [5–7]. While industrial processes vary in detail, they generally involve two key stages: VAC polymerization and monomer separation/recovery. Methanol, used as a solvent during polymerization, necessitates strict control of reaction rates to ensure product quality. However, significant amounts of unpolymerized VAC remain, requiring energy-intensive separation and recovery processes that consume large quantities of methanol [8–11]. This separation step not only directly impacts product quality but also significantly affects overall production energy efficiency and economic viability. The methanol–VAC azeotropic system presents substantial challenges in separation. Current methods include azeotropic distillation, extractive distillation (ED), and pressure swing distillation [12]. However, traditional azeotropic distillation struggles to efficiently separate this system even with added entrainers. Consequently, in international industrial production, ED is commonly employed to handle this system [13,14]. ED has gained widespread acceptance in the chemical industry due to its operational simplicity and

* Corresponding authors.
E-mail addresses: buctlqs@126.com (Q. Li), 20200043@immu.edu.cn (Y. Li).

https://doi.org/10.1016/j.cjche.2025.06.004

effectiveness in separating azeotropic mixtures [15–17]. The fundamental principle of this technique involves adding a specific extractive agent to the azeotropic system, thereby significantly enhancing the relative volatility of the components and enabling effective separation of the azeotrope [18–20]. In practical industrial applications, ED has been successfully utilized for the separation of various azeotropic systems, such as ethanol–water and methanol–acetone. For instance, Li and Bai [21] proposed a three-column ED process, comprising an ED column, a solvent recovery column, and a concentrator, for the separation of the ethanol–water system. By simulating and optimizing the process using Aspen Plus software, the researchers determined the optimal operating parameters, which demonstrated significant energy-saving advantages of the process. Additionally, Wang *et al.* [22] developed an ED process using sulfolane as the extractive agent for the separation of aromatic and non-aromatic azeotropic systems. By incorporating flash drums and decanters, the researchers optimized the reboiler heat load of the solvent recovery column. Compared to the existing optimal ED process, the newly proposed process achieved an 8.9% reduction in energy consumption costs. Pressure swing distillation (PSD) is an advanced technique for azeotropic separation that leverages changes in pressure to alter the composition and boiling points of azeotropes, thereby breaking the azeotropic point and enabling effective component separation. This technology is particularly suitable for azeotropic systems that are highly sensitive to pressure changes, especially when a pressure variation induces a composition change of over 5% in the azeotrope. One of the key advantages of PSD is that it does not require the introduction of a third component, such as an entrainer or extractive agent. This simplifies the process flow and avoids the additional energy consumption and product contamination associated with the use of separation media, making PSD a promising technique for azeotropic separation. In terms of specific applications, Yang *et al.* [23] proposed a three-column PSD process for the separation of the azeotropic mixture of *n*-propanol, tetrahydrofuran, and water. To address the high energy consumption associated with PSD, the study combined azeotropic distillation with PSD and employed a sequential iteration method to optimize the process. Furthermore, the integration of heat integration technology and heat pump energy-saving technology minimized energy consumption. Moreover, You *et al.* [24] introduced an environmentally friendly and energy-saving PSD process through a systematic approach. This method utilized temperature–composition diagrams to preliminarily determine the operating pressure and separation sequence, and evaluated the sustainability of the process by minimizing the total life cycle cost. The application of heat integration and heat pump technologies further enhanced energy savings and process sustainability. Compared to azeotropic and ED, PSD not only simplifies the process by eliminating the need for a third component but also effectively reduces energy consumption through heat coupling. Studies have shown that for the same binary azeotropic system, PSD can save more energy than conventional azeotropic distillation when pressure changes significantly affect the azeotropic composition [25–27]. This makes PSD an efficient, energy-saving, and environmentally friendly separation method with broad application prospects [28,29].

The present study investigates the materials of methanol–VAC ED and methanol recovery process in the polyvinyl alcohol operation department of a chemical enterprise. The energy maximization utilization (MEU) network mathematical model is adopted for the research, in conjunction with the energy-saving technology of heat exchange in the middle of distillation. The Aspen process simulation software is employed to conduct a comprehensive analysis of the methanol–VAC system. The primary focus of the research is the investigation of the PSD system, with the aim of assessing its feasibility in this context and identifying the key process parameters through detailed process simulation of the PSD separation process. The study is expected to provide substantial data support and a theoretical foundation for the PSD process in the methanol–VAC system.

2. Steady State/Dynamic Control and Energy Saving Optimization Strategy of Energy Network Based on Mathematical Model

2.1. Construction of mathematical model for steady state control of distillation

In Aspen Plus, steady-state simulation, which assumes that the process is at equilibrium with all operational variables and process parameters remaining constant over time, serves as the foundation. This type of simulation is particularly valuable for predicting and optimizing material and energy balances during the design phase and in existing production processes.

Aspen Plus employs the sequential modular approach for computational convergence. This method is based on unit modules, which typically correspond one-to-one with process units. These unit modules are subprograms developed based on the mathematical models and solution algorithms of the respective process units and have a unidirectional characteristic. Starting from the system feed stream, calculations are performed sequentially through each unit module. The output stream variables from one unit module serve as the input variables for the next adjacent unit. This sequential calculation continues until the system's output streams are determined, yielding all stream variables (*i.e.*, state variables) within the process system. Typically, input stream variables and unit module parameters (*e.g.*, reflux ratios, geometric dimensions) are used as decision variables. The sequential modular approach is closely related to the structure of the process system. For systems with feedback connections (non-separable subsystems), tearing and convergence techniques are necessary. For example, consider the simple process flow diagram shown in Fig. 1. Stream S1, together with stream S4 from the outlet of module C, enters module A and produces stream S2. Stream S2 then passes through module B to generate stream S3, which subsequently enters module C to produce streams S5 and S4. The equation sets for modules A, B, and C (outputs S4) are denoted as F1, F2, and F3, respectively. As illustrated, S2, S3, and S4 form a loop. According to the tearing rules of the sequential modular method, S4 is torn for iteration. In the simulation, S4 is divided into the output result S4 and the initial value S4'. Initially, S4′ is assigned an initial value, and calculations are performed according to each module's rules to obtain the output result S4.

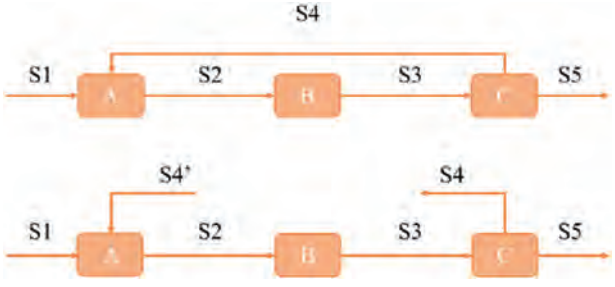

Fig. 1. Sequential module fracture rule.

$$S2 = F1(S4', S1) \quad (1)$$

$$S3 = F2(S2) \quad (2)$$

$$S4 = F3(S3) \quad (3)$$

$$S3 = F2[F1(S4', S1)] \quad (4)$$

$$S4 = F3\{F2[F1(S4', S1)]\} \quad (5)$$

In the sequential modular approach, the result S4 is compared with the initial value S4′. If the error between them is less than ε (the iteration tolerance), the iteration is successful. If the error exceeds ε, the initial value for the second iteration is set to the result of the first iteration, and a new result is calculated. This process repeats until the error is within the tolerance. This method is known as direct iteration in the sequential modular approach, with the specific iteration criteria illustrated in Fig. 2.

2.2. Construction of mathematical model for dynamic control of distillation

In industrial practice, distillation systems are often affected by various disturbances, such as fluctuations in feed flow rate and changes in feed composition. To precisely control the quality of the distillate and maintain operational stability, Aspen dynamics process simulation software provides valuable theoretical guidance and practical reference. By simulating dynamic processes, it helps optimize operational parameters, enhance production efficiency, ensure consistent product quality, and thereby strengthen market competitiveness.

2.2.1. Mathematical model for dynamic control of tower kettle

The dynamic control system is designed to fully account for the influence of time parameters on the operating process. Specifically, as shown in Fig. 3, the dynamic process on the heating medium side of the reboiler can be expressed as follows:

$$\frac{dT_R}{dt} = w_R(\Delta H F_{in} - Q_R) \quad (6)$$

And the dynamic process of reboiler heat load is

$$\frac{dQ_R}{dt} = F_R K_R S_R \left[\frac{dT_R}{dt} - \frac{1}{2}\left(\frac{dT_W}{dt} + \frac{dT_N}{dt}\right)\right] \quad (7)$$

where the parameters are: Q_R (kJ) is reboiler heat load; T_R (K) is reboiler temperature of the heating medium; w_R is reboiler correlation coefficient; F_R (kmol·s^{-1}) is reboiler flow rate of the vapour; K_R is reboiler heat transfer coefficient; S_R (m^2) is reboiler heat transfer area; T_W (K) is the kettle temperature; T_N (K) is temperature of the last plate; ΔH (kJ·kmol^{-1}) is latent heat of vaporization of steam.

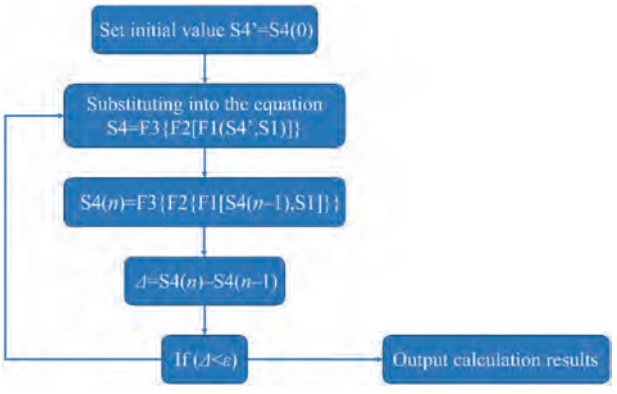

Fig. 2. Iterative process of sequential module method.

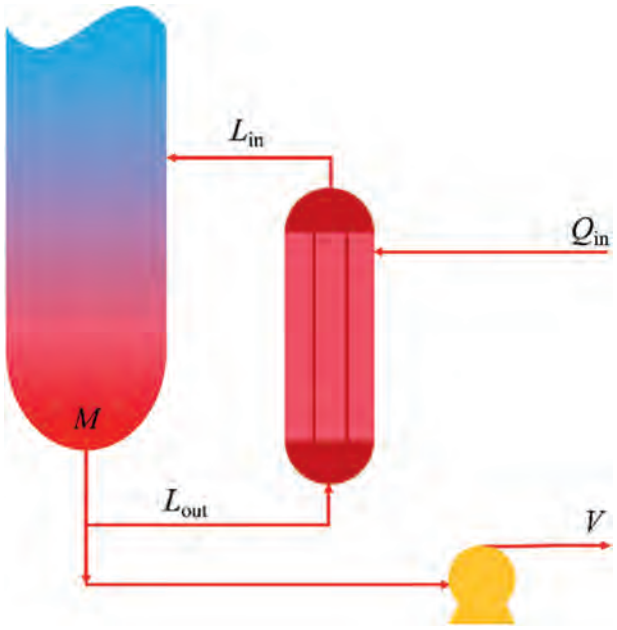

Fig. 3. Diagram of reboiler and kettle extraction.

Materials accountancy:

$$\frac{dM}{dt} = L_{in} - L_{out} - V \quad (8)$$

Energy accountancy:

$$\frac{d\left(MH^L\right)}{dt} = L_{in}H^L - L_{out}H^L - VH^V + Q_{in} \quad (9)$$

Associative Eqs. (8) and (9) are collapsed to give:

$$\frac{dH^L}{dt} = \frac{Q_{in} - V\left(H^L + H^V\right)}{M} \quad (10)$$

where the parameters are: M (kmol·s^{-1}) is volume of liquid held in the tower kettle; H^L (kJ·kmol^{-1}) is specific enthalpy of the liquid

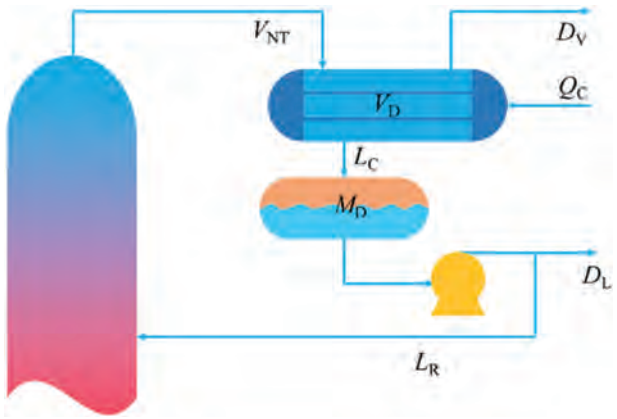

Fig. 4. Diagram of condenser and reflux drum.

phase; H^V (kJ·kmol^{-1}) is specific enthalpy of the vapour phase; Q_{in} (kJ·s^{-1}) is heat input; L_{in} (kmol·s^{-1}) is liquid phase flow rate into the tower kettle; L_{out} (kmol·s^{-1}) is liquid phase flow rate out of the autoclave.

2.2.2. Mathematical modelling of tower top dynamic control

As shown in Fig. 4, materials accountancy for the top reflux tank of the tower:

$$\frac{dM_D}{dt} = L_C - L_R - D_L = \frac{Q_C}{\Delta H_V} - L_R - D_L \tag{11}$$

where the parameters are: M_D (kmol·s^{-1}) is liquid holding capacity of the reflux tank; L_C (kmol·s^{-1}) is flow rate of the liquid phase in the condenser; L_R (kmol·s^{-1}) is flow rate of liquid phase reflux; D_L (kmol·s^{-1}) is flow rate of liquid phase extraction; Q_C (kmol·s^{-1}) is cooling input; ΔH_V (kJ·kmol^{-1}) is latent heat of vaporization.

For tower top pressure:

$$\frac{V_{Drum}}{RT_R}\frac{dp}{dt} = V_{NT} - L_C - D_V = V_{NT} - \frac{Q_C}{\Delta H_V} - D_V \tag{12}$$

where the parameters are: V_{Drum} (kmol·s^{-1}) is flow rate of the vapour phase in the reflux tank; T_R (K) is temperature of the condenser; R (J·kmol^{-1}·K^{-1}) is ideal gas constant; V_{NT} (kmol·s^{-1}) is vapour phase flow rate from the first plate into the condenser; D_V (kmol·s^{-1}) is flow rate of vapour phase extraction.

Laplace transformation of Eqs. (11) and (12):

$$P_{(S)} = \left[\frac{-\frac{RT_R}{V_{Drum}\Delta H_V}}{S}\right] Q_{C(S)} + \left[\frac{-\frac{RT_R}{V_{Drum}\Delta H_V}}{S}\right] D_{V(S)} + [0]L_{R(S)} \tag{13}$$

$$M_{D(S)} = \left[\frac{\frac{1}{\Delta H_V}}{S}\right] Q_{C(S)} + [0]D_{V(S)} + \left[\frac{-1}{S}\right] L_{R(s)} + [0]L_{R(S)} \tag{14}$$

where $S = a + b\hat{i}$ is a complex number.

From the above analysis, it can be seen that the liquid level of the reflux tank is related to the condenser load and reflux flow rate at the top of the tower, and the liquid level of the reflux tank is related to the liquid-phase extraction, not related to the vapour-phase extraction; the pressure at the top of the tower is related to the condenser load and vapour-phase extraction.

2.3. Construction of a MEU model for multi-scale, multi-objective optimization

The distillation process is a high-energy consuming part of chemical production. By establishing a mathematical model, the operating parameters of the distillation column (*e.g.* reflux ratio, temperature at the top of the column, temperature at the bottom of the column, *etc.*) can be optimized so as to reduce energy consumption. In the chemical separation process, there are complex and dynamic energy exchanges between key units, such as separation equipment and heat exchangers, at different time and space scales. In order to optimize this process systematically, a multi-scale and multi-objective MEU network model is proposed in this paper. The model aims to simultaneously optimize the energy recovery efficiency, equipment investment costs and environmental impacts to achieve sustainable development of chemical processes.

The present study focuses on the distillation column, a key chemical unit, and constructs a comprehensive multi-objective optimization framework by considering several key operating parameters (*e.g.* distillate flow rate, reflux ratio, theoretical number of plates, number of feed plates, *etc.*). The employment of advanced multi-objective optimization algorithms, such as genetic algorithms (GA) and particle swarm optimization (PSO), facilitates the global optimization of the distillation process. These algorithms adeptly balance competing objectives, thereby identifying optimal solutions that satisfy diverse optimization criteria.

The multi-dimensional optimization analysis of this study provides theoretical guidance for the energy coupling between distillation columns and heat exchange equipment, with the objective of maximizing heat recovery efficiency and consequently achieving a significant reduction in energy consumption within the context of the chemical process. This, in turn, enables the realization of the overarching goal of energy saving and consumption reduction. Furthermore, the multi-scale characteristics of the model enable it to adapt to the energy exchange characteristics in different time and space scales, thereby further enhancing the universality and practicality of the model.

As shown in Fig. 5, Q_{ik}^H is the heat load of logistics i entering at temperature interval k, which can be expressed as

$$Q_{ik}^H = F_i \times (C_p)_{ik} \times \Delta T_{ik} \tag{15}$$

where the parameters are: F is mass flow rate; C_p is heat capacity in a certain temperature interval; ΔT is temperature difference in a certain temperature interval.

Q_{jk}^C is the load of cold flow j with the outflow temperature interval k, which can be expressed as

$$Q_{ik}^C = F_j \times (C_p)_{jk} \times \Delta T_{jk} \tag{16}$$

Q_{mk}^S is the load of the thermal utility logistics m entering the temperature interval k, which can be expressed as

$$Q_{mk}^S = F_m^S \times \Delta h_{mk} \tag{17}$$

where the parameters are: F^S is mass flow rate of utility logistics; ΔT is enthalpy change of utility logistics in a certain temperature interval.

Q_{nk}^w is the load of cold utility logistics n for outflow temperature interval k, which can be expressed as

$$Q_{nk}^W = F_n^W \times \Delta h_{nk} \tag{18}$$

The total energy balance equation is then

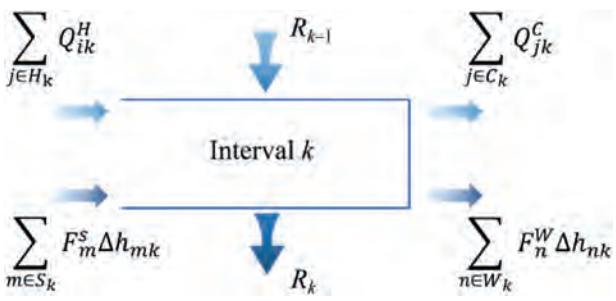

Fig. 5. Heat flow diagrams for each temperature interval.

$$R_k - R_{k-1} + \sum_{n\epsilon W_k} F_n^W \times \Delta h_{nk} - \sum_{n\epsilon S_i} F_n^S \Delta h_{nk} = \sum_{i\epsilon H_i} Q_{ik}^H - \sum_{j\epsilon C_i} Q_{jk}^C \tag{19}$$

where R is residual heat at the outflow temperature interval.

The cost of utility work is

$$Z = \sum_{m\epsilon S} S_m \times F_m^s + \sum_{n\epsilon W} W_n \times F_n^W \tag{20}$$

where the parameters are: S is thermal utility work pool; S_m is unit price of hot utility work; W is cold utility work collection; W_n is unit price of cold utility work.

Then the linear programming problem for the lowest utility cost is

$$\text{Minimize } Z = \sum_{m\epsilon S} S_m \times F_m^s + \sum_{n\epsilon W} W_n \times F_n^W \tag{21}$$

S.t.

$$R_k - R_{k-1} + \sum_{n\epsilon W_i} F_n^W \times \Delta h_{nk} - \sum_{m\epsilon S_i} F_n^S \Delta h_{nk} = \sum_{i\epsilon H_i} Q_{ik}^H - \sum_{j=C_i} Q_{jk}^C \tag{22}$$

where there is no residual flow inflow for the first temperature interval and no residual flow outflow for the last interval, so R_0=$R_k = 0$.

Assuming that there are (NL−1) pinch points in the system, the whole process is divided into NL sub-networks, and the corresponding subset of temperature intervals for each sub-network can be denoted as SNL, with $l = 1, 2 \cdots$, NL. The matching of heat transfer between streams has to be confined within each sub-network, otherwise the pinch points will have energy passing through them, *i.e.*, increase the amount of utility work.

The objective function for the lowest number of heat transfer units is

$$\text{Minimize } N = \sum_{i=1}^{\text{NL}} \sum_{i\epsilon H_i} \sum_{j\epsilon C_i} e_{ijl} \times Y_{ijl} \tag{23}$$

S.t.

$$R_k - R_{k-1} + \sum_{j\in C_{lk}} Q_{ijk} = Q_{ik}^H \tag{24}$$

$$\sum_{i\in H_{lk}} Q_{ijk} = Q_{jk}^C \tag{25}$$

$$\sum_{k\in \text{SNL}} Q_{ijk} = Q_{jk}^C \tag{26}$$

$$\sum_{k\in \text{SNL}} Q_{ijk} - U_{ijk} Y_{ijk} \le 0 \tag{27}$$

where the parameters are: e_{ijl} is the priority degree of matching heat transfer between logistics, generally can be taken as 1; Y_{ijl} is whether the matching heat transfer between hot logistics i and cold logistics j exists in the sub-network; when the hot and cold logistics are matched, $Y = 1$, when the hot and cold logistics cannot be matched, $Y = 0$; U_{ijk} is the upper bound of possible heat exchange, *i.e.* $\min\left\{\sum_{k\in \text{SNL}} Q_{ik}^H, \sum_{k\in \text{SNL}} Q_{jk}^C\right\}$.

In summary, the operating and equipment costs of the system are weighed and the network with the lowest total cost is selected as the final heat transfer network.

2.4. Modelling of techno-economic benefits

The total annual cost (TAC) is commonly employed for evaluating the economic viability of chemical separation processes. Consequently, this study adopts the minimization of TAC as the optimal outcome. The detailed calculation method for TAC was obtained by consulting relevant literature [30] and has been widely applied in the field. The expression for TAC is presented in Eq. (28)

$$\text{TAC} = \text{TIC} + \text{TOC} \tag{28}$$

In the equation, total installed cost (TIC) represents the annual equipment cost, which only considers the main equipment of the distillation system, including the tower shell, trays, and heat exchangers. The costs of reflux drums, pumps, and valves are neglected due to their insignificance compared to those of the tower and heat exchangers. Total operating cost (TOC) represents the annual operating cost, which only considers the expenses of heating steam, cooling water, and electricity consumption.

Table 1 presents the detailed formula for calculating the TAC. For tower equipment costs, the tower height is determined based on the number of trays, with an inter-tray spacing of 0.61 m. The tower diameter is obtained from Aspen Plus software. Once the tower height and diameter are determined, the main equipment cost of the tower can be calculated. For heat exchanger cost calculations, the simulation results provide the thermal loads. The heat transfer coefficients are set at 0.852 $\text{kW}\cdot\text{m}^{-2}\cdot\text{K}^{-1}$ for the condenser and 0.568 $\text{kW}\cdot\text{m}^{-2}\cdot\text{K}^{-1}$ for the reboiler. The heat transfer area is calculated based on the temperature difference, which allows for the determination of the heat exchanger equipment cost.

The unit prices for different steam pressures are as follows: low-pressure steam (160 °C) at 7.72 $\text{USD}\cdot\text{GJ}^{-1}$, medium-pressure steam (184 °C) at 8.22 $\text{USD}\cdot\text{GJ}^{-1}$, and high-pressure steam (260 °C) at 9.88 $\text{USD}\cdot\text{GJ}^{-1}$. The formula for calculating steam costs is shown in Table 1.

In Table 1, for calculating the tower body equipment cost factor (F_C), F_C=$F_m \times F_P$, where $F_m = 3.67$ and F_P is obtained from Table 2. For the tower tray equipment cost F_C, F_C=$F_S + F_t + F_m$, with $F_S = 1.0$, $F_t = 0$ (for sieve trays), and $F_m = 1.7$. For the heat exchanger cost F_C, $F_C = (F_d + F_P) \times F_m$, where $F_m = 3.75$, $F_d = 1.35$ (for reboilers), $F_d = 0.8$ (for fixed-tube-sheet heat exchangers), and F_P is from Table 3. Q_R and Q_C (kW) are the reboiler and condenser duties, λ_V ($\text{kJ}\cdot\text{kg}^{-1}$) is the latent heat of vaporization, and C_S ($\text{USD}\cdot\text{kg}^{-1}$) is the heating steam cost. M&S denotes the Marshall & Swift cost index, set at 1638.2.

3. Results and Discussion

3.1. Feasibility submissions

In this study, a distillation dynamic control mathematical model, a MEU network model and a techno-economic efficiency model were combined to optimize the separation process of a methanol–VAC system with the aid of Aspen Plus. The accuracy of the Aspen Plus process simulation is contingent on the accuracy of the thermodynamic phase equilibrium calculations, and the choice of physical properties method and the reliability of the binary interaction parameters are directly related to the accuracy of the simulation results.

The methanol–VAC system, being a polar system devoid of electrolytes, necessitates reliable gas–liquid phase interaction parameters for the purpose of simulation. The thermodynamic methods most frequently applied to this system include the Wilson,

Table 1
TAC calculation formula.

Items		Calculation formulas	
Equipment cost/USD·a^{-1}	Tower height	$H = 1.2 \times 0.6096 \times (N_T - 2)$	(29)
	Tower equipment cost	$C_1 = \left(\frac{M\&S}{280}\right) \times 937.636 \times ID^{1.066} \times H^{0.802} \times (2.18 + F_C)$	(30)
	Tray equipment cost	$C_2 = \left(\frac{M\&S}{280}\right) \times 97.243 \times ID^{1.55} \times H \times F_C$	(31)
	Heat transfer area of condenser	$A_C = \frac{Q_C}{K_C \Delta T_C}$	(32)
	Condenser cost	$C_3 = \left(\frac{M\&S}{280}\right) \times 474.668 \times A_C^{0.65} \times (2.29 + F_C)$	(33)
	Reboiler heat transfer area	$A_R = \frac{Q_R}{K_R \Delta T_R}$	(34)
	Reboiler cost	$C_4 = \left(\frac{M\&S}{280}\right) \times 474.668 \times A_R^{0.65} \times (2.29 + F_C)$	(35)
Operating cost/USD·a^{-1}	Steam	$C_s = \frac{Q_R}{\lambda_V} \times 3600 \times 8000$	(36)

Table 2
Values of F_P in tower cost calculation.

Pressure/kPa	≤344.505	689.01	1378.02
F_P	1.00	1.05	1.15

Table 3
The value of F_P in tray cost calculation.

Pressure/kPa	≤1033.515	2067.03	2756.04	5512.08
F_P	0.00	0.10	0.25	0.52

NRTL, and UNIQUAC physical methods. The Wilson and NRTL methods are characterized by a broad range of applicability and high computational accuracy. However, the Wilson method is unable to calculate activity coefficients at liquid–liquid equilibrium, rendering it unsuitable for liquid–liquid layered systems. Conversely, the UNIQUAC method is more appropriate for systems with significant molecular size disparities. The NRTL property method is particularly well-suited for the simulation of the methanol–VAC system, due to its applicability in liquid–liquid equilibrium calculations and its capacity to accurately describe polar systems.

PSD is a method of achieving effective separation by shifting the azeotropic point of an azeotropic system by changing the operating pressure. The key prerequisite for its application is that the azeotropic point can be disappeared by adjusting the pressure within a reasonable pressure range, or the molar fraction of the components in the azeotropic composition can be changed by more than 5%. The boiling points, azeotropic temperatures and azeotropic compositions of methanol–VAC systems at varying pressures have been calculated by the NRTL method and are displayed in Table 4.

As shown in Table 4, an experiment was conducted to ascertain the effect of pressure on the azeotropic composition. It was found that there was a decrease in the content of VAC of 13.93% when the pressure increased from 30 to 500 kPa. This indicates that the azeotrope belongs to the system that is more sensitive to pressure changes. Furthermore, it has been demonstrated that VAC does not undergo polymerization even when subjected to heating conditions below 120 °C and in the absence of oxygen [5,6]. Consequently, based on thermodynamic and kinetic analyses, the methanol–VAC system is deemed to be a viable candidate for azeotropic separation through the implementation of PSD.

3.2. Construction of PSD process flow

PSD is a specialized distillation technique that utilizes the principle of regulating the azeotropic composition of azeotropes by varying the pressure to achieve an efficient separation process. The selection of the operating pressure is a pivotal factor in the context of PSD. On the one hand, it is essential to assess the extent to which the pressure change affects the azeotropic composition; on the other hand, it is also necessary to take into account the pressure resistance of the equipment to avoid excessive pressure. It is imperative to note that elevated pressure levels can potentially result in an escalation in the financial outlay required for the acquisition of the necessary equipment. Conversely, inadequate pressure may have a deleterious effect on the efficiency of separation processes, thereby exerting a negative influence on the overall operational costs. Consequently, it can be deduced that the selection of an optimal operating pressure constitutes the fundamental prerequisite for ensuring the economic and efficient operation of PSD processes.

In accordance with the principle of PSD, it is imperative to augment the pressure differential between the two towers to the greatest extent possible within a reasonable range. This approach is conducive to enhancing the separation efficiency of azeotropes. As illustrated in Table 4, the operating pressure of the low-pressure column can be set at 30 kPa, resulting in an azeotropic temperature of 31.08 °C. This condition allows for the condenser at the tower's summit to be cooled using chilled water. When considered in conjunction with the gas–liquid equilibrium curves of the methanol–VAC system at varying pressures, as illustrated in Fig. 6, it is evident that the azeotropic composition undergoes a lesser degree of alteration when the pressure is elevated from 400 to 800 kPa. Consequently, the operating pressure of the high-pressure column can be selected to be 400 kPa, at which time the azeotropic temperature is 100.23 °C. Based on these findings, the gas phase at the top of the high-pressure column can be used as the heat source of the low-pressure column, and if the heat is insufficient, 400 kPa steam can be used additionally.

The composition of the material to be separated is shown in Table 5. In view of the fact that the feed contains only small amounts of light components, such as acetaldehyde, a condenser is installed at the top of the low-pressure column to achieve effective removal of these light components. Furthermore, due to the minimal water content in the feed, the moisture content of methanol in the autoclave of the low-pressure column is marginally higher than anticipated. Consequently, the crude methanol from the autoclave necessitates additional transportation to the recovery tower for distillation.

As illustrated in Fig. 6 the designed methanol–VAC PSD process flow is characterized by the following parameters: an operating pressure of 30 kPa for the low-pressure column and 400 kPa for the high-pressure column. The feed stream S1, having undergone preheating in the heat exchanger, is amalgamated with the recycle stream extracted from the uppermost level of the high-pressure column, subsequently entering the low-pressure column in unison. The crude methanol extracted from the nadir of the low-pressure

Table 4
Boiling point, azeotropic temperature and azeotropic composition at different pressures.

Pressure/kPa	Boiling points/°C		Azeotropic temperature/°C	Azeotropic mass composition/%	
	Methanol	VAC		Methanol	VAC
30	36.51	40.31	31.08	34.84	65.16
40	42.65	47.33	37.32	35.87	64.13
100	64.19	72.29	59.30	39.59	60.41
150	74.88	84.93	70.21	41.52	58.48
200	82.84	94.58	78.45	43.01	56.99
300	94.99	109.18	90.82	45.36	54.64
400	104.07	120.51	100.23	47.20	52.80
500	111.21	129.82	107.91	48.77	51.23

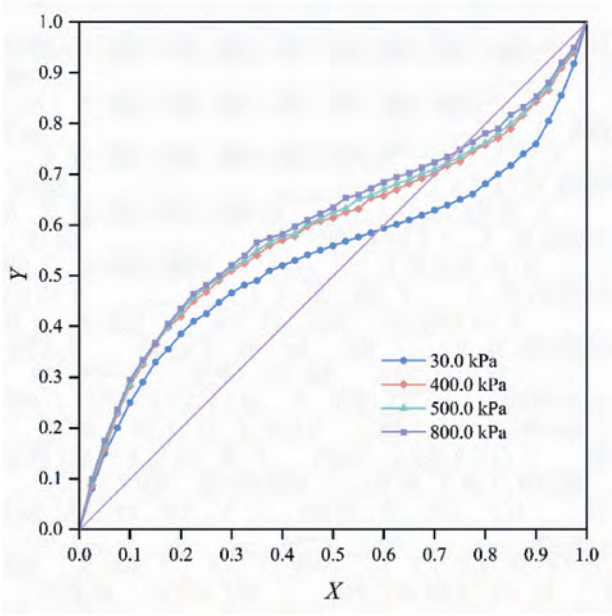

Fig. 6. Methanol–VAC gas–liquid equilibrium diagrams at different pressures (*X*/*Y* represents the molar content of methanol in the liquid/gas phase).

column is amalgamated with the crude methanol derived from the other units, and is directed towards third recovery tower for the purpose of further separation of the methanol from the minor quantity of water. Concurrently, the methanol–VAC azeotrope at this pressure is extracted in liquid phase at the top of the low-pressure column, and this material, after mixing with the VAC from the other units, enters the high-pressure column. Due to the change in pressure, the azeotropic composition also changes. In the high-pressure column, the composition of stream S9 at the tower's summit is proximate to the azeotropic composition at the novel pressure. Refined VAC is withdrawn *via* a sidestream in the medial and inferior regions of the tower, and the polymerization inhibitor is taken at the tower's base.

As shown in Table 6, the fluctuations introduced by initialization are minimal, and the deviation between the steady-state initial results and the dynamic initial results is negligible. Consequently, this study prioritizes the use of Aspen Plus steady-state simulation due to its computational efficiency and simplicity.

3.3. Pressure swing distillation process simulation and optimization analysis

3.3.1. Simulation model construction

In this study, an in-depth analysis of the proposed scheme was conducted using Aspen Plus process simulation software, and the specific simulation process is shown in Fig. 7. In the simulation process, the RadFrac model was selected for all distillation columns and the heater model was employed for the heat exchangers. The NRTL physical property method was employed for the simulation calculations, and the mass fractions of the separated products, VAC and methanol, were specified to be not less than 99.7% and 99.6%, respectively.

3.3.2. Synergistic study of sensitivity analysis and parameter optimization

During PSD, the composition of the feed from the top of the reducing and high-pressure column approximates the azeotropic composition at their respective operating pressures. Given that the feed to the high-pressure column originates from the top of the low-pressure column, it is possible to set the feed composition and temperature of the high-pressure column to the azeotropic composition and azeotropic temperature at the operating pressure of the low-pressure column. The primary parameters influencing the separation efficacy and energy consumption of the high-pressure column encompass the theoretical number of plates, the feed position, the reflux ratio, and the side mining position. Given the nature of methanol–VAC as a homogeneous azeotrope, the DSTWU module is not applicable for estimating parameters such as the theoretical number of plates and the minimum reflux ratio necessary for distillation. Consequently, the present study has opted for a sensitivity analysis of the aforementioned operating parameters, employing the Aspen Plus software to ascertain the most optimal process parameters.

In the selection of the sidestream withdrawal position in the high-pressure column, the reflux mass ratio was initially set to 0.58, the feed position was determined as the theoretical number of trays minus 11, and the sidestream position was set to the theoretical number of trays minus 4, with all other process parameters maintained at their original values. The sidestream position was optimized by prioritizing regions within the column where the gas phase exhibited a high concentration of VAC and the liquid phase contained minimal polymerization inhibitor, thereby ensuring that the VAC purity in the sidestream met the technical specifications while optimizing steam consumption and capital expenditure. Subsequently, the theoretical number of trays in the high-pressure column was adjusted to examine its impact on steam usage and the VAC content in the sidestream, with the results illustrated in Fig. 8. The study demonstrated that adjusting the theoretical number of trays could significantly reduce steam consumption while maintaining separation efficiency, thereby enhancing the economic viability and sustainability of the process.

As demonstrated in Fig. 8, when the number of theoretical plates is less than 27, the content of side-mined VAC increases significantly with the increase of the number of theoretical plates, while the steam usage decreases rapidly. However, when the number of theoretical plates exceeds 27, the changes in the

Table 5
Composition of feed after initial process treatment of methanol–VAC.

Item		Methanol –VAC	Other units VAC	Recovery of crude methanol from second tower	Recovery of crude methanol from forth tower	Depolymerization agent
Volume/t·h^{-1}		24.9	1.22	9.02	7.42	0.33
Mass composition/%	Water	0.6	1.40	79.79	11.73	
	Methyl acetate		1.00	0.003	3.6×10^{-4}	
	Methanol	42.0		20.18	88.26	
	Acetaldehyde	0.2			3.8×10^{-8}	
	VAC	57.1	96.60		Trace	
	Acetone	0.1				
	Benzoquinone		1.00			

Table 6
Comparison between the steady-state initial results and the dynamic initial results.

Item	Low-pressure column			Item	High-pressure column		
	Steady-state initial value	Dynamic initial value	Deviation/ %		Steady-state initial value	Dynamic initial value	Deviation/ %
Top temperature/°C	33.598	33.598	0.000	Top temperature/°C	99.615	99.615	0.000
Kettle temperature/°C	48.125	48.128	0.006	Kettle temperature/°C	128.069	128.068	−0.001
Top of the tower distillation/ t·h^{-1}	14.3200	14.3201	0.001	Top of the tower distillation/ t·h^{-1}	14.0600	14.0601	0.001
Tower bottom $w(CH_3OH)$/%	91.6510	91.6601	0.001	Side-stream $w(CH_3OH)$/%	2.2307	2.2307	0.000
Tower bottom w(VAC)/%	2.0720	2.0718	−0.010	Side-stream w(VAC)/%	94.6102	94.6168	0.007

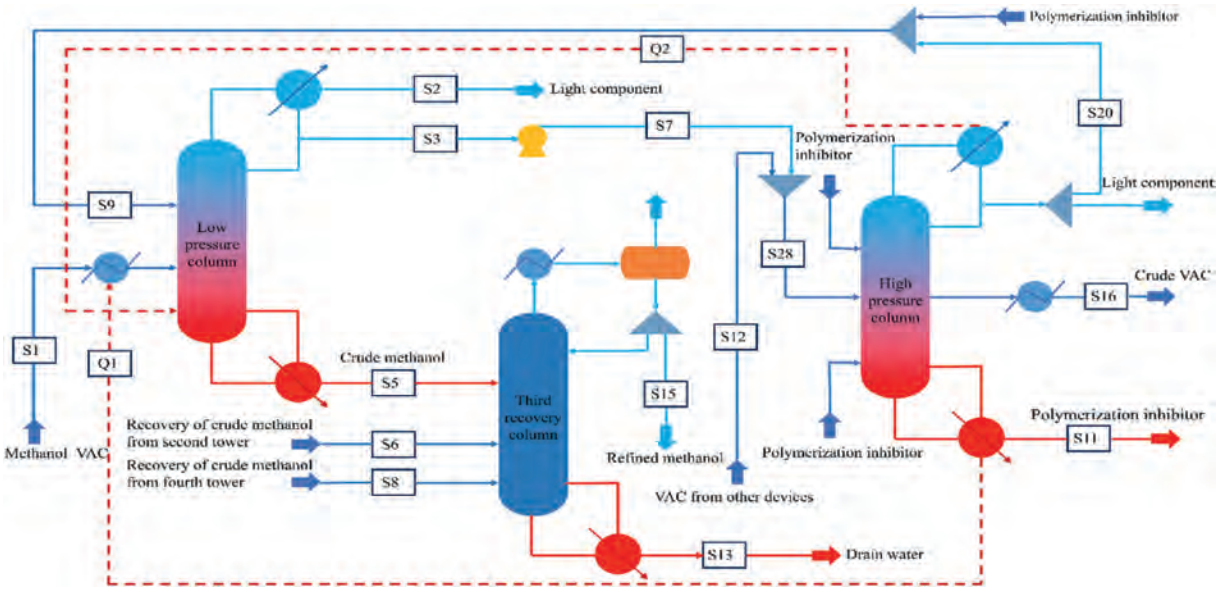

Fig. 7. Methanol–VAC PSD process flow.

content of side-mined VAC and steam usage stabilize and no longer fluctuate significantly. The separation efficiency and equipment cost were taken into consideration, and it was determined that the optimum number of theoretical plates for the high-pressure column was 28.

Under these conditions, it was found that the mass content of VAC could reach 99.7%, while the steam usage was kept at a low level. The effects of feed position on product quality and steam consumption were investigated further, under the premise of setting the theoretical number of tower plates to 28 and keeping other parameters unchanged. The results of the simulation analysis are shown in Fig. 9.

As observed in Fig. 9, a gradual downward shift in the feed position of the high-pressure column resulted in a slow increase and subsequent sharp decrease in the mass fraction of VAC extracted from the side. The underlying reason for this phenomenon can be attributed to the fact that, when the feed position is situated close to the apex of the tower, the theoretical number of plates within the distillation section is found to be minimal, thereby hindering effective separation. Conversely, when the feed position is in close proximity to the kettle, the theoretical number of plates within the distillation section is also found to be minimal, which is also detrimental to the separation process. Furthermore, the downward shift of the feed position results in an increase in

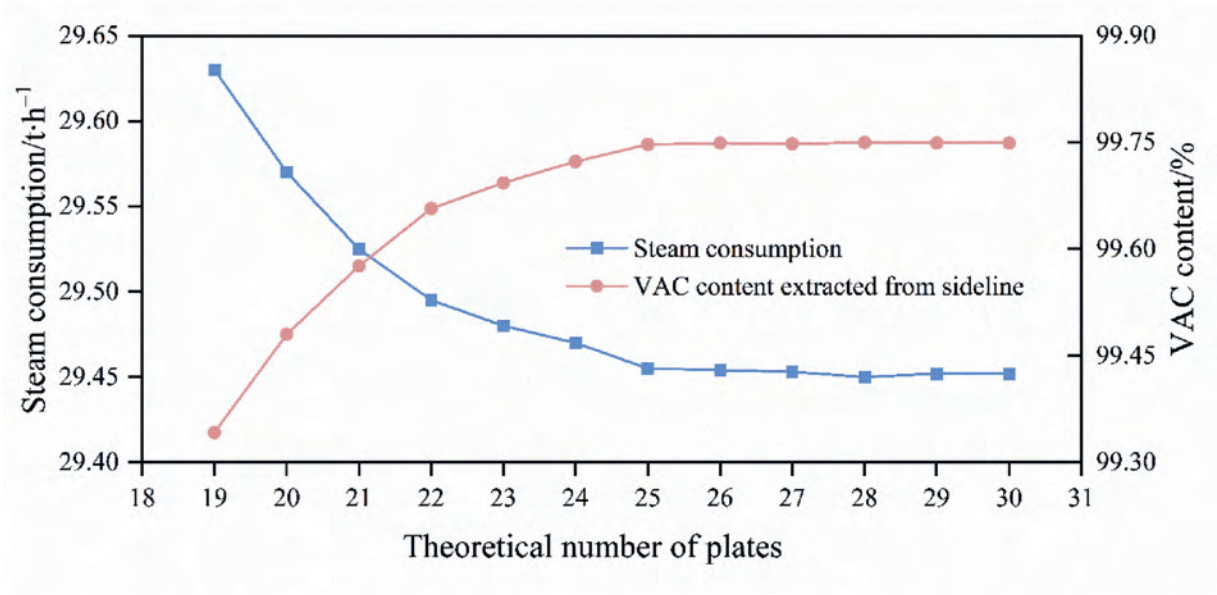

Fig. 8. Impacts of theoretical plate number of high-pressure column on vapour pressure and VAC mass content extracted from sideline.

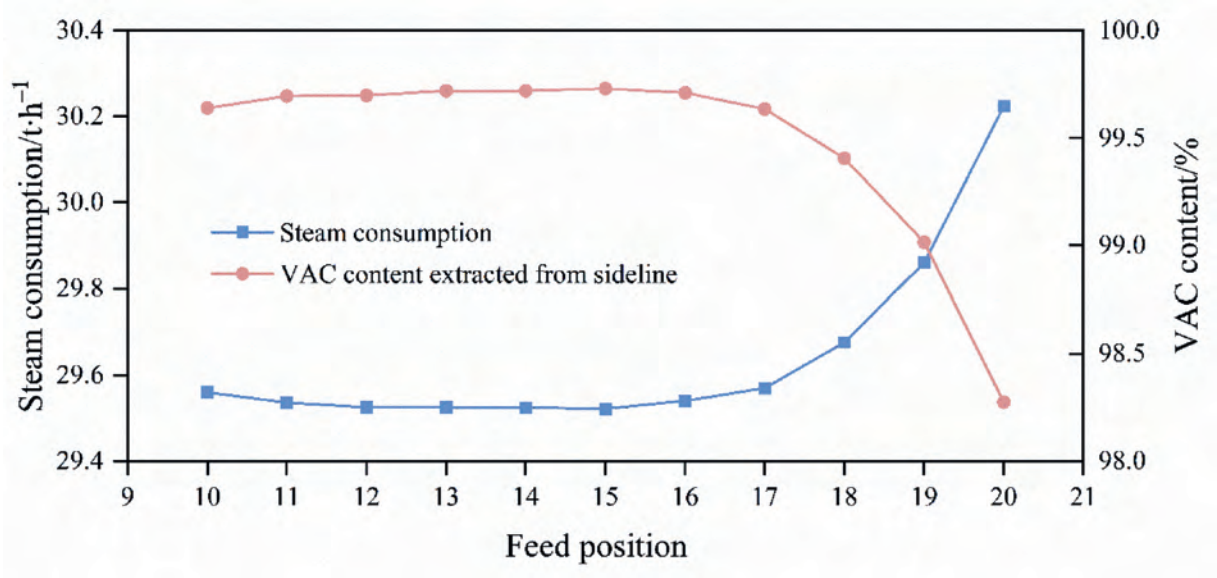

Fig. 9. Impacts of high-pressure column feed location on steam pressure and VAC mass content extracted from sideline.

the load on the reboiler. However, with a feed position between 13 and 16 theoretical plates, the mass fraction of VAC extracted from the side was able to meet the established separation requirements. Considering the separation index and energy consumption, the optimal feeding position of the high-pressure column is determined to be the 15th theoretical plate. At this point, the VAC mass content in the sidetracked material reached its highest value of 99.73%.

In the simulation process, the number of theoretical plates was set to 28 plates, and the 15th theoretical plate was selected as the feed plate. Under the premise of ensuring that other operating parameters remain constant, the influence of reflux ratio on product quality and steam consumption was investigated in depth, and the relevant simulation results are shown in Table 7. After analyzing the data in Table 7, it can be found that increasing the reflux ratio significantly improves the product quality. However, an increase in the reflux ratio will also lead to an increase in the load of the gas and liquid phases in the tower, which in turn will increase the load on the reboiler. The simulation results demonstrate a rapid increase in the content of VAC in the side-mined material with an increase in the reflux ratio, followed by a gradual stabilization of the change pattern. When the objective is to ensure a VAC content in the sidetracked material of 99.73%, it can be concluded that, under the condition of a reflux ratio of 0.55, the load borne by the reboiler is relatively small.

The extraction of the product from the sideline is known to result in the production of VAC, thereby directly impacting product quality and energy consumption. Setting the number of theoretical plates at 28, the feed position at the 15th theoretical plate, and the reflux ratio at 0.55, the influence of the position of the

Table 7
Influence of return flow rate on the quality of sideline of VAC.

Reflux ratio	Number of theoretical plates	Feed position	VAC mass fraction/%	Steam consumption/t·h^{-1}
0.30	28	15	96.83	27.592
0.35	28	15	97.36	28.465
0.40	28	15	97.70	28.876
0.45	28	15	98.59	29.054
0.50	28	15	99.64	29.351
0.55	28	15	99.73	29.522
0.60	28	15	99.66	29.972

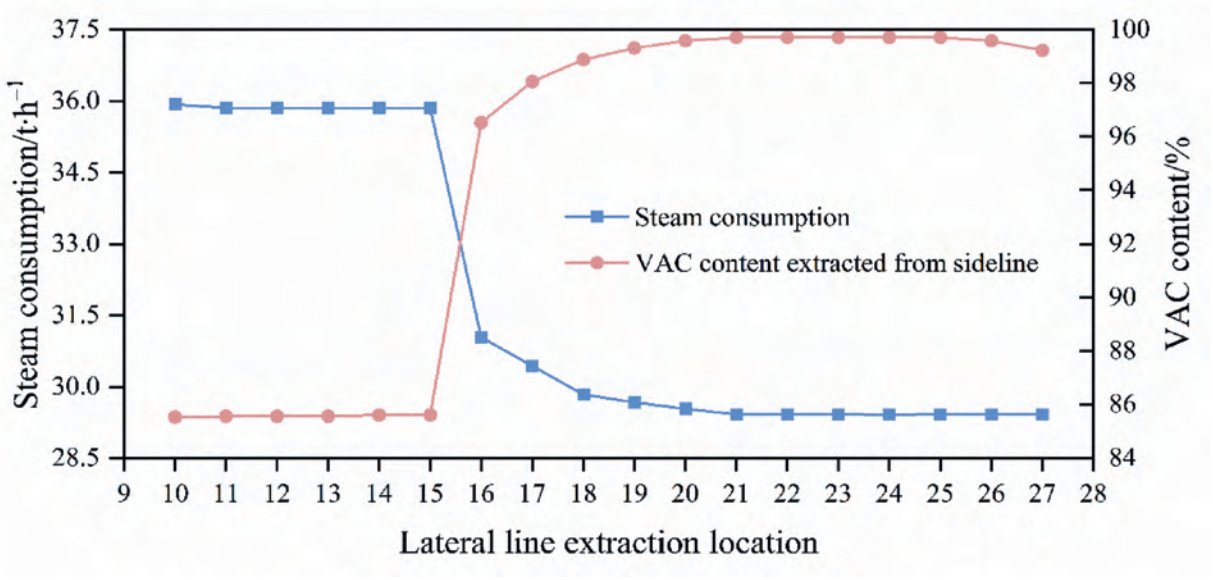

Fig. 10. Impacts of high-pressure column sidetracking location on steam usage and VAC mass content extracted from sideline.

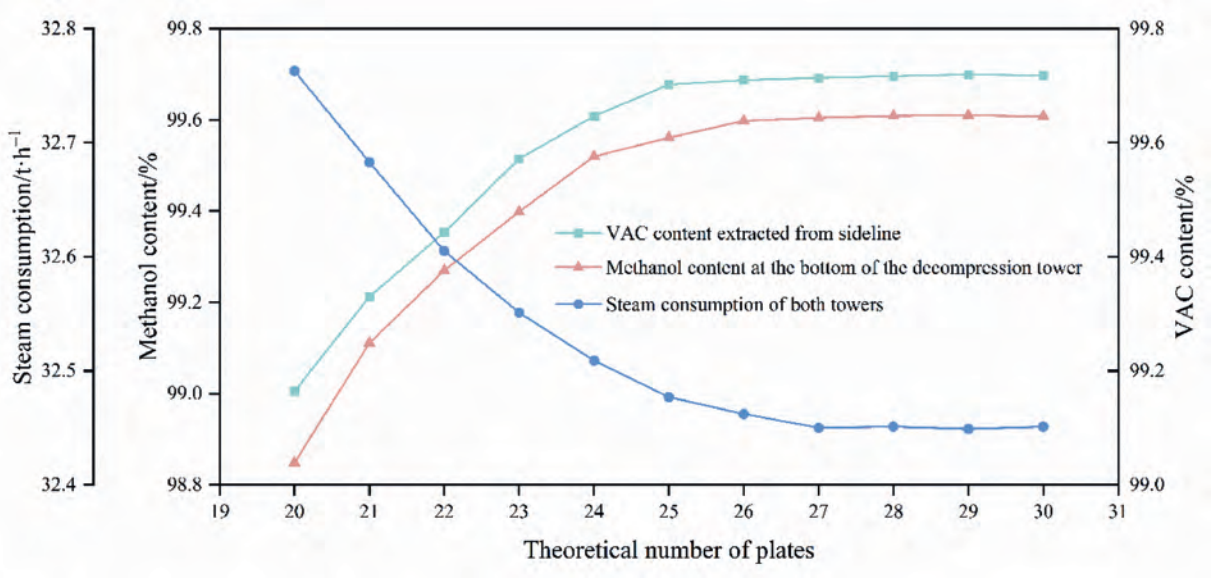

Fig. 11. Impacts of the theoretical plate number of a low-pressure column on the main indexes.

sideline extraction on product quality and steam consumption was investigated further. The results of the related simulation analyses are shown in Fig. 10.

As demonstrated in Fig. 10, the 15th theoretical plate is designated as the feed plate, and the section of the tower above the feed plate is designated as the distillation section. This section

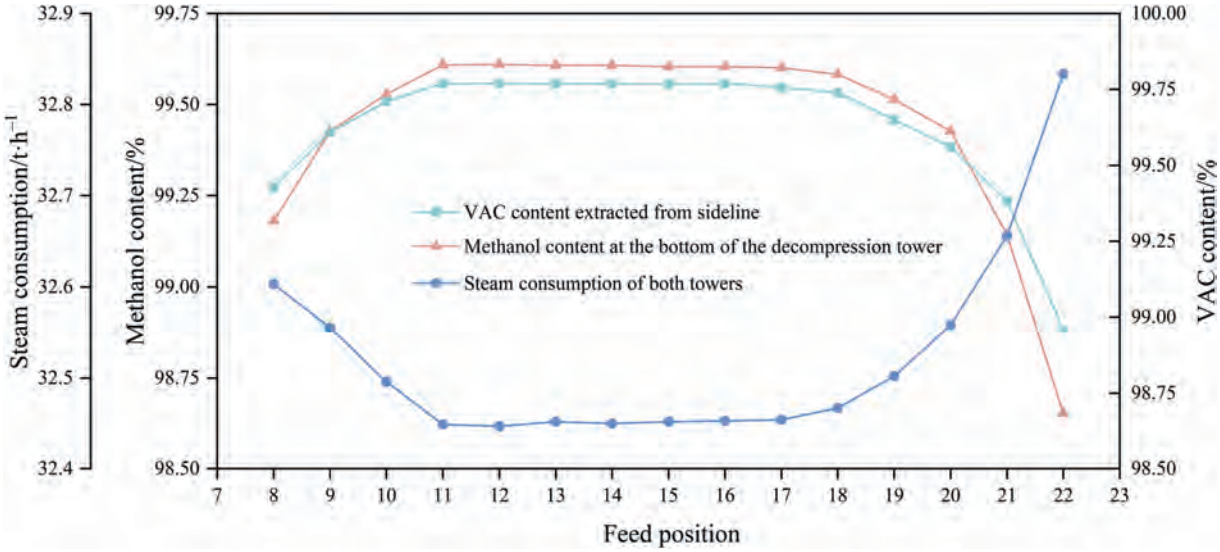

Fig. 12. Impacts of low-pressure column feed position on key indicators.

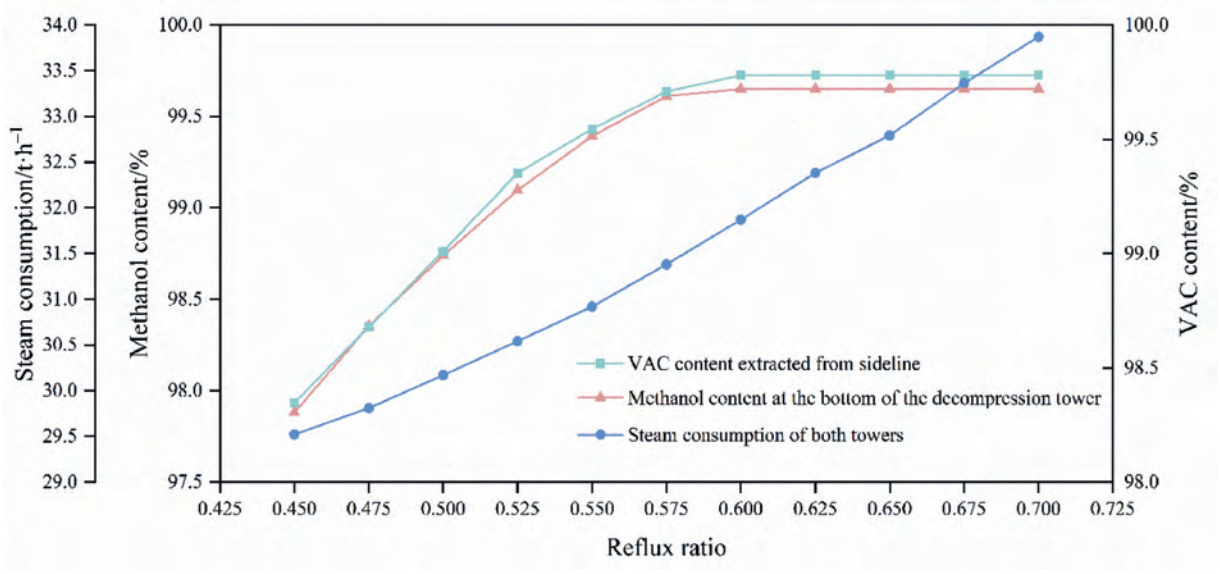

Fig. 13. Impacts of low-pressure column reflux ratio on key indicators.

Table 8
Process parameters for low-pressure and high-pressure columns.

Tower	Theoretical plate number	Feed plate	Pressure at the top of the tower/kPa	Reflux ratio	Lateral mining position
Low-pressure column	29	12	30	0.625	
High-pressure column	28	15	400	0.55	24

primarily contains the light components of the feed and the methanol–VAC azeotrope. Conversely, the section of the tower below the feed plate is designated as the lifting section, which is responsible for thickening the recombined components. In the case of the sidetracking position being situated below the 15th theoretical plate, the content of VAC in the sidetracking material is found to be minimal, and there is negligible change in its content upon alteration of the sidetracking position. However, when the sidetracking position is situated above the 15th theoretical plate, the content of VAC in the sidetracking material increases rapidly, and subsequently stabilizes in the vicinity of the kettle position.

In consideration of the fact that the VAC recovered from the high-pressure column will be utilized in the polymerization reaction, it is imperative to minimize the content of polymerization inhibitor in the sidetracked material. Furthermore, given that the polymerization reaction of VAC is liquid phase polymerization, it is more appropriate to adopt the gas phase extraction method in the sideline. The optimal extraction location for the

sideline is thus determined to be the 24th theoretical plate, as evidenced by the analyses conducted.

In the chemical production process, the separation effect of the low-pressure column is influenced by several key parameters. In addition to the theoretical plate number, feed position and reflux ratio of these common factors, the circulation volume is also a significant parameter that cannot be disregarded. Given the direct impact of the low-pressure column's separation effect on the quality of products extracted from the side of the high-pressure column, it is imperative to consider the impact of each parameter on the main indicators of both the low-pressure and high-pressure columns concurrently when optimizing the operating parameters of the low-pressure column. The sensitivity analysis process of the low-pressure column is analogous to that of the high-pressure column. Specifically, the effects of the theoretical number of plates, the feed position and the reflux ratio of the low-pressure column on the main indexes are shown in Figs. 11–13, respectively.

A comprehensive analysis of the data from Figs. 11–13 was conducted to determine the optimum process parameters of the low-pressure column. The following parameters were determined to be optimal: the number of theoretical plates was 29, the feed position was located in the 12th theoretical plate, and the reflux ratio was set at 0.625. This finding was then corroborated by the simulation calculation of methanol–VAC distillation under variable pressure, which was undertaken to determine the optimum operating parameters of the low-pressure and high-pressure columns. The optimal operating parameters of the low-pressure and high-pressure columns are summarized in Table 8.

3.4. Simulation of the whole process of pressure swing distillation

The results of the optimization of the parameters of both the low-pressure and high-pressure columns were then used to conduct a full-flow simulation of the methanol–VAC PSD process. Given the critical role that the concentration distribution in the column plays in the design and operation of distillation columns, the mass fraction distribution of the gas and liquid phases in each theoretical plate in the low-pressure and high-pressure columns was studied in depth. The gas–liquid phase concentration distribution in the low-pressure column, the gas–liquid phase concentration distribution in the high-pressure column, and the results of the simulation of PSD are shown in Figs. 14 and 15 and Table 9, respectively.

As illustrated in Figs. 14 and 15, the gas–liquid phase composition at the summit of both towers approaches the azeotropic composition, attributable to the negligible presence of light components such as acetaldehyde in the feed. In the upper and middle regions of the tower, the mass fraction of gas–liquid phase components exhibit a more gradual change. For the lowest binary azeotrope, an increase in pressure results in an increase in the proportion of components with higher molar latent heat of vaporization in the azeotropic composition. Based on this principle, in the low-pressure column, the methanol content in the lower part of the tower increases rapidly and then levels off, while the VAC content in the middle and lower parts of the high-pressure column shows a rapid increase and then levels off. Furthermore, a slight decrease in VAC content in the liquid phase of the high-pressure column kettle is observed, attributable to the relative increase in polymerization inhibitor content in the kettle following the extraction of VAC from the gas phase of the sideline. In summary, the process of PSD allows the final methanol product to be obtained at the bottom of the high-pressure column, while the VAC product is extracted from the middle and lower sideline of the high-pressure column. As illustrated in Table 9, the methanol content of the methanol extracted from the bottom of the low-pressure column can reach up to 99.64% when employing the PSD process, and the resultant refined methanol can attain a purity level of 99.88% through straightforward treatment in the third recovery tower. Concurrently, the quality fraction of VAC extracted from the side of the high-pressure column can reach up to 99.73%, and the quality of these recovered products is found to fully meet the requirements of the technical indicators. As shown in Table 10, compared with ED in the literature [3–5], PSD can save 9.07 $t \cdot h^{-1}$ steam and reduce wastewater by 20.77 $t \cdot h^{-1}$.

As shown in Table 11, assuming a fixed capital payback period of 3 years and an annual operating time of 8000 h, the TAC of both the

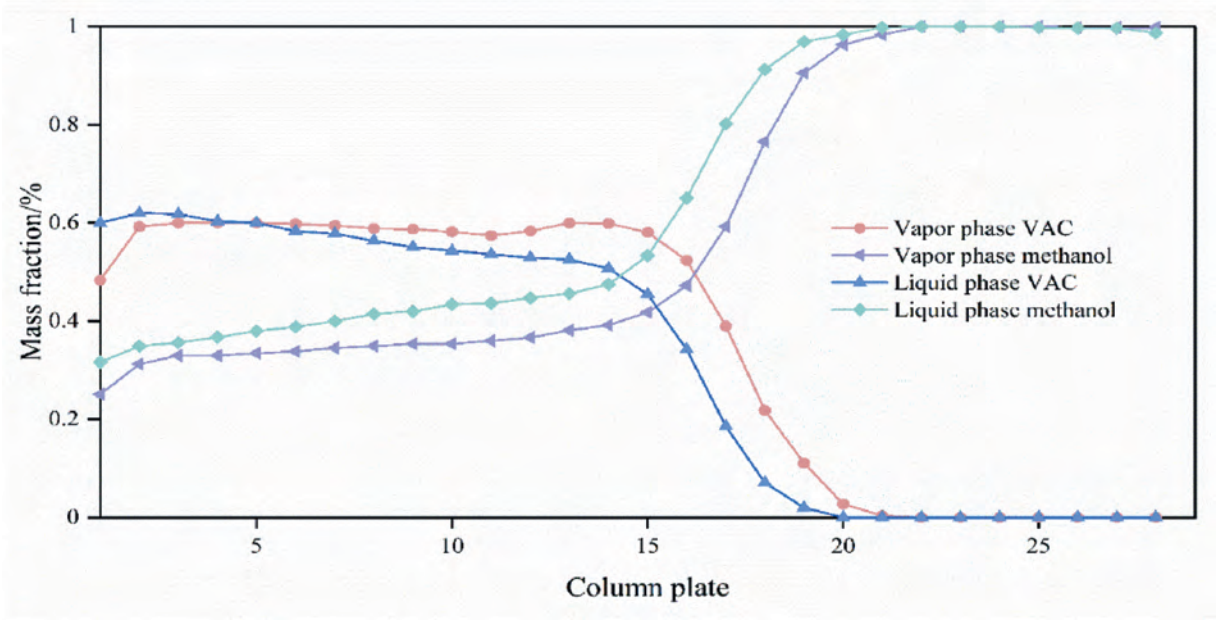

Fig. 14. Impacts of low-pressure column sidetrack location on steam usage and sidetrack VAC mass content.

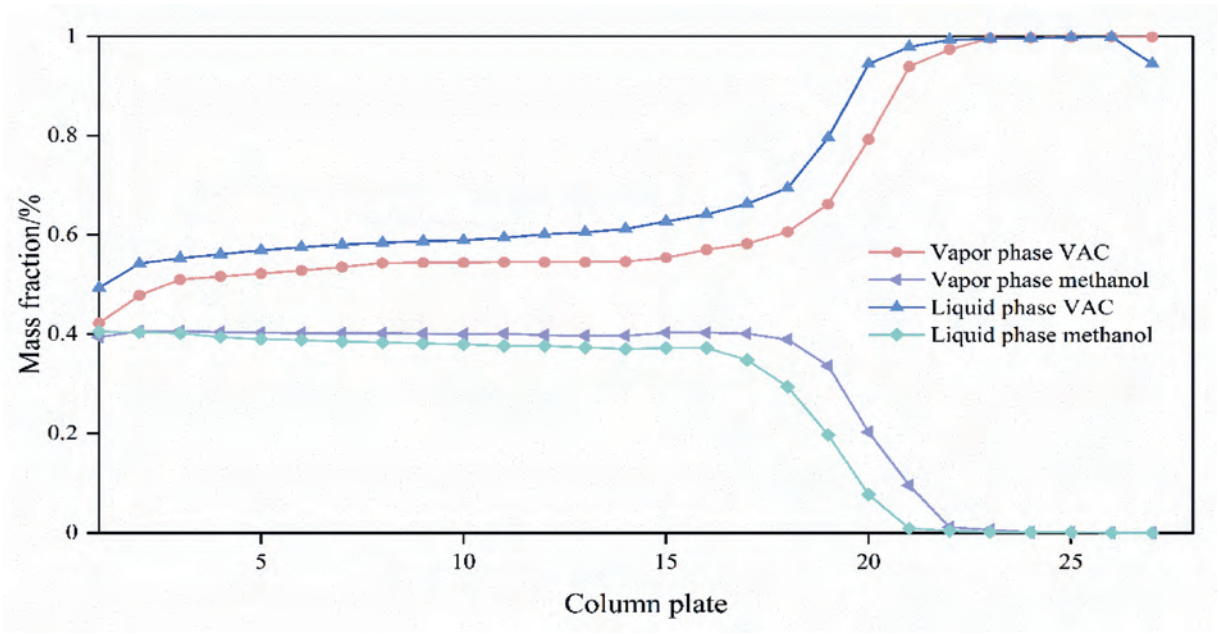

Fig. 15. Distributions of gas–liquid phase mass concentration in high-pressure column.

Table 9
Simulation results of PSD.

Item			Target	Simulation
Low-pressure column	Temperature at the top of the tower/°C			27.5
	Tower kettle temperature/°C			45.8
	Kettle composition/% (mass)	Water		0.16
		Methanol		99.64
		VAC		0.066
		Acetone		8.78×10^{-5}
		Benzoquinone		0.14
	0.4 MPa Steam consumption/t·h^{-1}			0.96
High-pressure column	Temperature at the top of the tower/°C			96.9
	Tower kettle temperature/°C			125.1
	Lateral line kettle composition/% (mass)	Water	≤0.04	3.7×10^{-5}
		Methanol		0.11
		Acetaldehyde	≤0.01	3.21×10^{-3}
		VAC	≥99.7	99.73
		Benzoquinone		0.001
	Tower kettle VAC/% (mass)			92.48
	Tower kettle benzoquinone/% (mass)			7.24
	0.4 MPa Steam consumption/t·h^{-1}			31.51
Third recovery tower	Temperature at the top of the tower/°C			98.9
	Tower kettle temperature/°C			140.3
	Tower top extraction composition/% (mass)	Water	≤0.2	0.08
		Methyl acetate	≤0.2	2.2×10^{-4}
		Methanol	≥99.6	99.88
		VAC		0.03
		Acetone		6.67×10^{-5}
	Tower kettle methanol/% (mass)		≤0.01	0.0018
	Tower kettle extraction/t·h^{-1}			8.25
	1.0 MPa Steam consumption/t·h^{-1}			26.83

Table 10
Comparison of steam usage and wastewater.

ED				PSD			
Steam consumption/t·h^{-1}			Waste water/t·h^{-1}	Steam consumption/t·h^{-1}			Waste water/t·h^{-1}
Second polymerization tower	Third polymerization tower	Second recovery tower		Low-pressure column	High-pressure column	Third recovery tower	
7.45	7.79	53.11	29.02	0.96	31.51	26.83	8.25

Table 11
Economic evaluation of the two options.

Items	ED	PSD
TIC/kUSD	5409.41	5239.87
TOC/kUSD	870.42	715.48
TAC/kUSD	2673.56	2462.11

ED process reported in the literature [3–5] and the differential pressure distillation process proposed in this study were calculated. The results indicate that the TAC of the differential pressure distillation process developed in this study achieved a 7.91% reduction compared to the ED process.

4. Conclusions

(1) The simulation of the methanol–VAC material system utilising the NRTL physical properties method has demonstrated its accuracy, reliability and effective application in the analysis and study of this azeotropic system.
(2) The pressure change exerts a significant effect on the system, with a concomitant decrease in the content of VAC in the azeotrope with increasing operating pressure. This outcome indicates that the azeotrope is a moderately pressure–sensitive system and is suitable for separation by PSD.
(3) The simulation calculation of the new methanol–VAC PSD process was carried out by using Aspen Plus software, and the results clearly showed that the PSD was able to achieve the effective separation of methanol–VAC, so that the mass fractions of methanol and VAC reached 99.88% and 99.73%, respectively.
(4) Furthermore, under the premise of ensuring product quality, the optimal operating parameters of each tower were determined as follows: the low-pressure column was equipped with 29 theoretical plates, with the feed position at the 12th theoretical plate and a reflux ratio of 0.625; and the pressurised tower had 28 theoretical plates, with the feed position at the 15th theoretical plate, a reflux ratio of 0.55, and the side extraction position at the 24th plate.
(5) Compared with ED reported in the literature PSD demonstrates significant energy and environmental benefits, reducing steam consumption by 9.07 $t \cdot h^{-1}$ and minimizing wastewater generation by 20.77 $t \cdot h^{-1}$.
(6) The results demonstrate that the TAC of the differential pressure distillation process developed in this study exhibits a superior economic performance, with a 7.91% reduction relative to the ED process reported in the literatur, as determined through detailed economic evaluation.
(7) The current study has completed Aspen Plus simulations for vacuum and high-pressure column conditions at 30 kPa and 400 kPa, respectively. Future work will expand to multi-pressure scenarios to evaluate energy consumption and economic performance. This research will aim to optimize industrial pressure ranges, balance key performance metrics, and provide theoretical insights and practical guidance for energy-efficient and sustainable separation process design.

Credit Authorship Contribution Statement

Xuefeng Feng: Writing – original draft, Software, Methodology, Investigation, Formal analysis, Conceptualization. Huiqin Zhou: Writing – original draft, Data curation. Yi Zhang: Visualization, Investigation. Shaolan Zhuang: Writing – review & editing. Zhongwei Ding: Supervision, Resources. Qunsheng Li: Writing – review & editing, Supervision, Resources, Funding acquisition, Conceptualization. Yuxin Li: Writing – review & editing, Supervision, Resources, Funding acquisition.

Declaration of Competing Interest

The authors declare no competing financial interest.

Acknowledgements

We are thankful for financial support from the National Key Research and Development Program of China (2022YFC2106300) and the National Nature Science Foundation of China (U2267226).

References

[1] C. Souza, J.X. Feng, A. Olah, G. Wnek, E. Baer, Thermoformable high oxygen barrier multilayer EVOH/LDPE film/foam, *J. Appl. Polym. Sci.* 137 (30) (2020) 48903.
[2] H.R. Zhang, Q. Zhao, M.J. Zhou, P.Z. Cui, Y.L. Wang, S.Q. Zheng, Z.Y. Zhu, J. Gao, Economic effect of an efficient and environmentally friendly extractive distillation/pervaporation process on the separation of ternary azeotropes with different compositions, *J. Clean. Prod.* 346 (2022) 131179.
[3] S. Nakamura, Solubility curve and liquid–liquid equilibrium of vinyl acetate–methanol water system and separation of vinyl acetate from vinyl acetate methanol mixtures by extraction, *J. Soc. Chem. Ind. Jpn.* 71 (3) (1968) 319–321.
[4] Z.Y. Zhu, X.L. Geng, W. He, C. Chen, Y.L. Wang, J. Gao, Computer-aided screening of ionic liquids as entrainers for separating methyl acetate and methanol *via* extractive distillation, *Ind. Eng. Chem. Res.* 57 (29) (2018) 9656–9664.
[5] J. Camacho, E. Díez, I. Díaz, G. Ovejero, Vapor–liquid equilibrium at p/kPa = 101.3 of the binary mixtures of ethenyl acetate with methanol and butan-1-ol, *J. Chem. Eng. Data* 57 (11) (2012) 3198–3202.
[6] L.J. Krolikowski, Feasible separation regions for distillation with ternary systems: an algorithm, *Ind. Eng. Chem. Res.* 59 (41) (2020) 18579–18594.
[7] Y. Su, A. Yang, S.M. Jin, W.F. Shen, P.Z. Cui, J.Z. Ren, Investigation on ternary system tetrahydrofuran/ethanol/water with three azeotropes separation *via* the combination of reactive and extractive distillation, *J. Clean. Prod.* 273 (2020) 123145.
[8] S.R. Sun, W. Chun, A. Yang, W.F. Shen, P.Z. Cui, J.Z. Ren, The separation of ternary azeotropic mixture: thermodynamic insight and improved multi-objective optimization, *Energy* 206 (2020) 118117.
[9] C. Jaksland, Internal Report on JOULE Project JOU2- R, Technical University of Denmark, Lyngby, 1996.
[10] A. Yang, W.F. Shen, S.A. Wei, L.C. Dong, J. Li, V. Gerbaud, Design and control of pressure-swing distillation for separating ternary systems with three binary minimum azeotropes, *AIChE J.* 65 (4) (2019) 1281–1293.
[11] J.S. Lee, K.H. Choi, H. Do Ghim, S.S. Kim, D.H. Chun, H.Y. Kim, W.S. Lyoo, Role of molecular weight of atactic poly(vinyl alcohol) (PVA) in the structure and properties of PVA nanofabric prepared by electrospinning, *J. Appl. Polym. Sci.* 93 (4) (2004) 1638–1646.
[12] Y.H. Yu, C.Y. Lin, J.M. Yeh, W.H. Lin, Preparation and properties of poly(vinyl alcohol)–clay nanocomposite materials, *Polymer* 44 (12) (2003) 3553–3560.
[13] G. Miao, K.S. Zhuo, G.Q. Li, J. Xiao, An advanced optimization strategy for enhancing the performance of a hybrid pressure-swing distillation process in effective binary-azeotrope separation, *Sep. Purif. Technol.* 282 (2022) 120130.
[14] X.H. Li, Q. Ye, Y.G. Xu, L.J. Chen, J.L. Li, Analysis and performance enhancement of heat pump technology assisted pressure-swing distillation process in the separation of azeotropic mixtures, *Chem. Eng. Process. Process Intensif.* 178 (2022) 109037.
[15] F.K. Zhang, D.F. Sun, Y.N. Li, B.M. Shan, Y.X. Ma, Y.L. Wang, X. Li, Z.Y. Zhu, Heat integration and dynamic control for separating the ternary azeotrope of butanone/isopropanol/*n*-heptane *via* pressure-swing distillation, *Chem. Eng. Process. Process Intensif.* 170 (2022) 108657.
[16] Y.R. Zhang, T.W. Wu, I.L. Chien, Energy-efficient heterogeneous azeotropic distillation coupling with pressure swing distillation for the separation of IPA/DIPE/Water mixture, *J. Taiwan Inst. Chem. Eng.* 130 (2022) 103843.
[17] J.M. Douglas, Conceptual Design of Chemical Processes, McGraw Hill, New York, 1988.
[18] C. Wang, Y. Zhuang, L.L. Liu, L. Zhang, J. Du, Heat pump assisted extractive distillation sequences with intermediate-boiling entrainer, *Appl. Therm. Eng.* 186 (2021) 116511.
[19] Y. Cui, X.J. Shi, C. Guang, Z.S. Zhang, C. Wang, C. Wang, Comparison of pressure-swing distillation and heterogeneous azeotropic distillation for recovering benzene and isopropanol from wastewater, *Process Saf. Environ. Prot.* 122 (2019) 1–12.

[20] X. Jian, J.L. Li, Q. Ye, L.Q. Yan, X.H. Li, J.Y. Zhang, Process synthesis of intensified extractive distillation for recycling organics material from wastewater, *Sep. Purif. Technol.* 303 (2022) 122172.
[21] G.Z. Li, P. Bai, New operation strategy for separation of ethanol−water by extractive distillation, *Ind. Eng. Chem. Res.* 51 (6) (2012) 2723−2729.
[22] Q. Wang, J.Y. Chen, M. Pan, C. He, C.C. He, B.J. Zhang, Q.L. Chen, A new sulfolane aromatic extractive distillation process and optimization for better energy utilization, *Chem. Eng. Process. Process Intensif.* 128 (2018) 80−95.
[23] A. Yang, Z.Y. Kong, J. Sunarso, W.F. Shen, Towards energy saving and carbon reduction of pressure-swing distillation for separating the ternary azeotropic mixtures by thermodynamic insights and process intensification, *Sep. Purif. Technol.* 301 (2022) 121983.
[24] X.Q. You, T.J. Ma, T. Qiu, Design and optimization of sustainable pressure swing distillation for minimum-boiling azeotrope separation, *Ind. Eng. Chem. Res.* 58 (47) (2019) 21659−21670.
[25] X.M. Qiu, M.J. Zhou, Z.Y. Zhu, J.G. Qi, Y.L. Wang, J.W. Yang, Comparative study on organic solvents and green solvents in separation of aromatic hydrocarbons/low-carbon alcohols azeotrope by structure−activity relationship, *Sep. Purif. Technol.* 297 (2022) 121498.
[26] F.S. Liu, Y. Hua, H. Wu, C.F. Lee, Z.M. Wang, Experimental and kinetic investigation on soot formation of *n*-butanol−gasoline blends in laminar coflow diffusion flames, *Fuel* 213 (2018) 195−205.
[27] T.S. Kumar, B. Ashok, Critical review on combustion phenomena of low carbon alcohols in SI engine with its challenges and future directions, *Renew. Sustain. Energy Rev.* 152 (2021) 111702.
[28] M.J. Zhou, K.X. Yin, D.C. Fan, K. Xue, J.X. Ruan, R.Y. Hu, Y.L. Wang, J.W. Yang, Phase behavior and internal micro mechanism of separation of extracting low-carbon alcohols fuel additive with green solvents, *Fuel* 366 (2024) 131413.
[29] P.Z. Cui, X.Y. Liu, F. Zhao, Z.Y. Zhu, L. Wang, Y.L. Wang, Molecular mechanism, thermoeconomic, and environmental impact for separation of isopropanol and water using the choline-based DESs as extractants, *Ind. Eng. Chem. Res.* 59 (36) (2020) 16077−16087.
[30] Q.S. Li, N. Hu, S.P. Zhang, Q.P. Wu, J. Qi, Energy-saving heat integrated extraction-azeotropic distillation for separating isobutanol−ethanol−water, *Sep. Purif. Technol.* 255 (2021) 117695.